Analytical Design of Practical-Thickness Slab Devices Supporting Bound States in the Continuum

Analytical Design of Practical-Thickness Slab Devices Supporting Bound States in the Continuum

Ovidiu-Zeno Lipan*, Aldo De Sabata†, Ladislau Matekovits†‡§
* Department of Physics, University of Richmond, Richmond, VA, USA
olipan@richmond.edu
†Department of Measurements and Optical Electronics, University Politehnica Timisoara, Timisoara, Romania
aldo.de-sabata@upt.ro
‡Department of Electronics and Telecommunications, Politecnico di Torino, Torino, Italy
§Istituto di Elettronica e di Ingegneria dell'Informazione e delle Telecomunicazioni, National Research Council of Italy, 10129 Turin, Italy
ladislau.matekovits@polito.it

***Abstract*—The use of bound states in the continuum (BICs) in photonic crystal slabs, which are Bloch eigenstates with zero linewidth and infinite lifetimes, facilitates the development of microwave resonators with ultrahigh quality factors and enhances antenna performance by enabling strong field confinement and radiation control. In this paper, we propose a method to design devices that sustain bound states in the continuum (BICs) for microwave applications. This method relies on a theoretical framework initially developed for thin photonic slabs. The objective of this study is to demonstrate that increasing the slab thickness, starting from a thin configuration, preserves the BIC properties of the device. This finding is significant for engineering microwave devices and antennas that support BICs while accommodating practical slab thicknesses that are not excessively small.**

***Index Terms*—bound states in the continuum, microwave devices, antenna design, slab thickness, Bloch-Floquet modes, resonance, high-Q resonators, electromagnetic theory**

I. Introduction

BOUND states in the continuum (BICs) represent an apparent paradox: electromagnetic modes remain confined within a material slab placed, say, in air, even though they are, in principle, allowed to escape into the surrounding air. In conventional scenarios, confined modes—such as those in a waveguide or cavity—correspond to states lying below a specific frequency threshold, which prevents them from coupling to radiative modes. In contrast, BICs challenge this expectation: their frequency lies within the continuum of propagating states, above the threshold, yet they remain localized in the vicinity of the slab, effectively behaving like non-radiating or evanescent-like modes. The concept traces back to quantum mechanics, where von Neumann and Wigner, in 1929, demonstrated that specially designed potentials could localize electron wavefunctions in non-radiative states, even when embedded within a continuum of extended states [1]. In electromagnetism, a parallel phenomenon occurs with electromagnetic waves: BICs emerge in periodic structures—such as photonic crystals, gratings, or metasurfaces—through mechanisms like destructive interference or symmetry protection [2], [3].

From a practical standpoint, photonic BICs are compelling because they can support extremely high quality factors (Q-factors), enabling enhanced performance in applications such as sensors and filters. These exceptional properties arise from different underlying mechanisms. For instance, symmetry-protected BICs occur when the symmetry of a mode is incompatible with that of the available radiating channels—preventing any coupling to outgoing waves. In contrast, interference-based (or 'accidental') BICs rely on precise tuning of structural parameters to achieve destructive interference that cancels all radiation leakage.

In a series of papers, the geometry of a crystal slab—the size and spacing of its holes—is engineered to realize bound states in the continuum (BICs) within a targeted frequency band. The key principle used to find the set of parameters is to make the transfer matrix of the device singular and, in addition, to ensure it has a specific singularity. The specific singularity is attained only after the elements of the transfer matrix can be computed in a closed analytical form, as only then does a formula for the singularity become derivable. The derivation of analytical formulas for the transfer matrix elements was accomplished by solving Maxwell's equations analytically [4], using the discrete-space formulation proposed by Pendry and MacKinnon. The discretization of space, which was crucial to the success of this approach, introduces a constraint: the thickness of each layer comprising the device must be smaller than the dimensions of the unit cell. Consequently, identifying the transfer matrix singularity within the vast parameter space of geometrical and material structures requires, as an initial step, the use of a device composed of thin laminae.

However, once the singular point is reached, there is no restriction against exploring the effects of increasing the lamina thickness, thereby moving beyond the realm of thin crystal slabs. This paper investigates precisely this objective, motivated by an interest in comparing the theoretical analytical formulas with the numerical results derived from the Finite Integration Technique (FIT) method through simulations.

II. The unit cell and the analytic formulas

The geometry of a device experimentally demonstrated to exhibit bound states in the continuum (BICs) is illustrated in Figure 1.

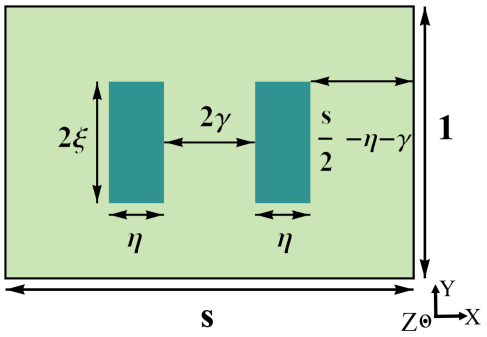

Fig. 1. The unit cell. The selected geometrical structure features two symmetrically positioned windows with a permittivity distinct from that of the surrounding background. All geometrical parameters are dimensionless and normalized by l_y, the vertical edge length of the unit cell. The unit cell is not required to be square, as indicated when $s \neq 1$. For this study, we choose to set $s = 1$.

It consists of a slab of material—silicon in this case, with a relative dielectric permittivity of 11.9—depicted in a light greenish color in Figure 1. Two windows, shown in dark green and separated by a distance of 2γ, contain a different material. In the present configuration, these windows are holes within the silicon background, resulting in a relative dielectric permittivity of 1. The length l_y of the unit cell's edge along the y-axis is defined as 1, serving as the reference length for formulating the equations. Consequently, the x-axis length of the unit cell is expressed as sl_y, while the x-axis lengths of the window edges are both equal to $2\xi ly$. Similarly, the y-axis length of the windows is given by ηl_y.

The class of quasi-bound states in the continuum (qBICs) we aim to excite in this device consists of symmetry-protected ones, activated by directing the incoming plane wave at $\theta \approx 0$ and $\varphi \approx 0$, corresponding to the vicinity of Γ point in the momentum space. For simplicity, we will maintain $\varphi = 0$ throughout the remainder of this paper. To ensure robust symmetry protection, we configure the unit cell as a square, setting $s = 1$ in Figure 1.

A set of sufficient conditions ensuring the unique type of singularity required to achieve bound states in the continuum (BICs) was first introduced in [5], with their significance elaborated upon below.

The singularity was realized in [5] by constraining the structure of the transfer matrix elements to either a symmetric or an antisymmetric configuration. For both imposed configurations, the following constraint relates the dimensions of the windows and their separation, 2γ, between them

$$\xi \sin(4\pi\gamma) - \xi \sin(4\pi(\gamma+\eta)) + \eta \sin(4\pi\xi) = 0. \quad (1)$$

A noteworthy observation is that this relation remains valid even when the two windows merge into a single one at $\gamma = 0$. This represents a continuous transition in the formula, yet it manifests as an abrupt transition in the device's structure. In addition, at one-windowed device, the above formula dramatically simplifies into

$$\mathrm{sinc}(4\pi\xi) = \mathrm{sinc}(4\pi\eta). \quad (2)$$

with $\mathrm{sinc}(x) = x^{-1}\sin(x)$. One evident solution is $\xi = \eta$, though a second curve exists in the ξ-η plane along which the equation also holds true. These curves are observed in Figure 2, on the plane $\gamma = 0$, where the entire surface described by Equation (1) is presented, including cases where $\gamma \neq 0$.

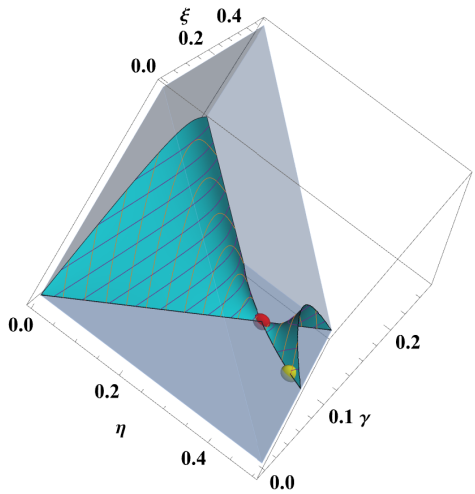

Fig. 2. Two devices are chosen based on the 3D surface that represents the first sufficient condition (1) for generating BICs. The SincSync point is colored red.

At the intersection of the two curves satisfying Equation (2), there lies a red-colored point in Figure 2, corresponding to $\xi = \eta = 0.358$. This device was comprehensively examined in [5], except for the effects arising from an increase in its thickness, which are addressed in the present study. The device, designated 'SincSync' in [5], is so named due to its precise location at the intersection of two distinct curves governed by the equation $\mathrm{sinc}(4\pi\xi) = \mathrm{sinc}(4\pi\eta)$.

A second device, indicated in yellow in Figure 2, will also be investigated in this study. The dimensions of this device are $\gamma = 0, \eta = 0,4648$ and $\xi = 0.27$. This second device features a single window that, unlike the square window of the red-colored point, is a quadrangle.

Traversing the curve defined by $\mathrm{sinc}(4\pi\xi) = \mathrm{sinc}(4\pi\eta)$ in the $\gamma = 0$ plane, from the red point to the yellow point, results in a smooth transformation of both the window's shape and the area occupied by the silicon, decreasing from 50.2% to 48.7%. Additionally, the window of this second device, where η is nearly twice as large as ξ, forms a ribbon-like region along the x-axis for the modes to propagate along. These two devices will be referenced either as the red-point and yellow-point devices or by their distinct (ξ, η) parameter pairs.

The second condition, which, together with Equation (1), forms a system of equations, establishes a relationship between the frequency, the permittivities, and the geometrical parameters is

$$\eta\xi(1+\text{sinc}(4\pi\xi)) = \frac{1}{4}\frac{((\epsilon_B-1)\Omega^2\Phi_e-1)^2-(\Phi_e)^2}{((\epsilon_B-1)\Omega^2\Phi_e-1)^2-1}. \quad (3)$$

The meanings of the symbols on the right-hand side of Equation (3) require discussion and context-specific clarification.

The permittivity ϵ_B characterizes the background silicon. The difference $\epsilon_B - 1$ represents the contrast between the background and the windows, which, in this paper, are filled with air, possessing a relative permittivity of 1.

Next, Ω is introduced as a dimensionless parameter representing the frequency, scaled by the device thickness L_z according to the following relationship:

$$\frac{\omega}{v_0} = 2\frac{\Omega}{L_z} = \frac{2\pi}{\lambda}, \quad (4)$$

where v_0 denotes the speed of light in a vacuum (equivalent to air in this context). This relation can also be utilized to link Ω with the wavelength, providing a valuable approach for correlating Ω with the dimensions of the unit cell.

In this paper, we adopt a frequency band in the tenths of GHz range, resulting in dimensions on the order of millimeters. More specifically, we set $L_y = 15$mm. Consequently, L_z, being smaller than L_y is chosen as, for example, $L_y/40$, yielding a value of $0.375\,$mm.

The final critical aspect of Equation (3), which determines the frequency band, requires an explanation of Φ_e. This term is, in fact, a function with an argument that is of great importance.

The Φ_e captures the propagation along the z-axes of evanescent waves, as described in [4]

$$\Phi_e = \Phi_{Z,\text{evanescent}}\left(\frac{1}{2}(2+w^2-\Omega^2)\right) \quad (5)$$

with

$$\Phi_{Z,\text{evanescent}}(z) = z - \sqrt{z^2-1} \quad (6)$$

$$w = l_z\pi. \quad (7)$$

It should be noted that l_z represents the dimensionless value of the thickness, scaled relative to L_y, such that $l_z = L_z/L_y$. For the case where $L_z = L_y/40$, this yields $w = \pi/40 = 0.0785$.

Equation (3) is now ready for use. For the yellow-point device shown in Figure 2, with $\eta = 0.4648$ and $\xi = 0.27, \epsilon_B = 11.9$, and the chosen value of $w = \pi/40 = 0.0785$, the solution for Ω is $\Omega = 0.07388$.

The argument $\left(\frac{1}{2}(2+w^2-\Omega^2)\right)$ yields a numerical value of 1.00035. This value, exceeding 1, ensures that the square root in Equation (6) is a real number, confirming that the bound states in the continuum (BICs) manifest as evanescent waves rather than propagating waves. In the latter case, Φ_e would become a complex number, as noted in [OpticsExpress].

The example we selected illustrates the design process utilizing Equation (1) initially, followed by Equation (3). This process begins with the selection of geometric parameters intended to position the bound states in the continuum (BICs) at a frequency near, but not equal to, 20 GHz, achieved by setting the unit cell dimensions 15 mm. Alternatively, the design can commence with Equation (3) by specifying the thickness of the crystal slab, the target frequency, and the material properties, subsequently determining the window dimensions through the application of Equation (1).

Prior to presenting the primary results, it is essential to address a significant aspect concerning the response of the device, which is constructed based on the design formulas outlined earlier.

As noted earlier, the transfer matrix elements exhibit two distinct patterns, manifesting at two separate frequencies, f_s and f_a. At f_s, where the pattern is symmetric, a pronounced resonance emerges as a dip in transmission. For instance, in Figure 3, this resonance is evident at $f = 18.48$ GHz. The subsequent two notches in the transmission spectrum signify the presence of two bound states in the continuum (BICs). The frequency of the resonance is governed by Equation (3), while the position of the BIC associated with the rightmost notch is determined by the same equation, albeit with its left-hand side modified to $\eta\xi(1-\text{sinc}(4\pi\xi))$.

The significant aspect emphasized earlier stems from the fact that these equations are formulated using a 5×5 transfer matrix, constructed from five Bloch-Floquet modes. When the number of modes is increased beyond five, a splitting occurs: instead of a single BIC, two BICs emerge, appearing as two distinct notches on the right side of the resonance. Notably, the resonance itself does not split, allowing us to track its behavior as the device thickness increases. The frequencies of the BICs demonstrate a consistent trend relative to the resonance, shifting toward lower values at a rate determined by the specific device configuration selected.

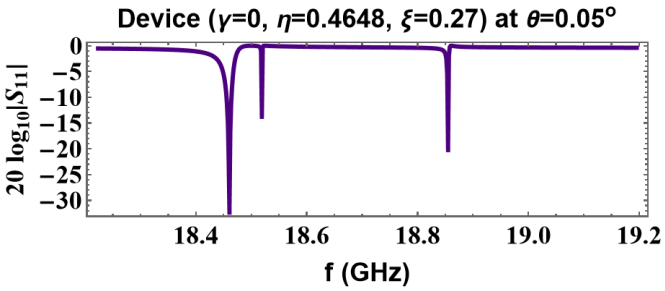

Fig. 3. The spectrum displays the resonance and bound states in the continuum for the yellow-point device at a thickness of $0.375\,$mm. Here, S_{11} denotes the scattering matrix element that characterizes the transmitted propagative mode.

III. Analysis of Thickness-Dependent Behavior in the Two Devices

The primary emphasis lies on the thickness of the devices, encapsulated within the w-parameter, which forms part of the argument of Φ_e, the z-function governing the evanescent Bloch-Floquet modes [OpticsExpress]. By solving Equation (3) for a variable w, we obtain the dependence $\Omega(w)$, distinct for each device—namely, the red-point and yellow-point devices depicted in Figure 2.

The close agreement between simulation and theoretical results serves as a promising indicator, particularly in light of the recommendation to design the device with thin layers.

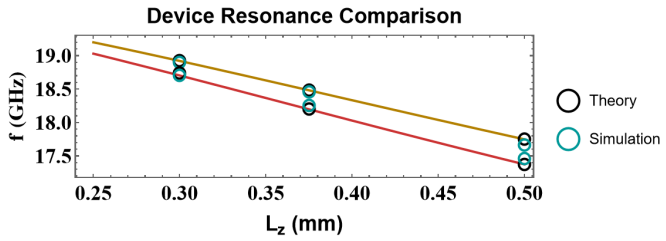

Fig. 4. Resonance of Red- and Yellow-Point Devices. The theoretical resonance positions for the red-point ($\xi = \eta = 0.358$) and yellow-point ($\xi = 0.27$, $\eta = 0.4648$) devices are indicated by the red and yellow lines, respectively. Transmission spectra reveal resonance shifts with increasing thickness. The rates of change differ, with values of $-6.62\,\text{GHz/mm}$ and $-5.80\,\text{GHz/mm}$ for the red-point and yellow-point devices, respectively.

This suggests that the desired design properties persist as the thickness increases, demonstrating that the theoretical framework remains valid even at greater thicknesses beyond the conservatively chosen initial values. This finding is significant, as practical considerations often require thicker devices, given that excessively thin configurations are susceptible to damage during installation or handling.

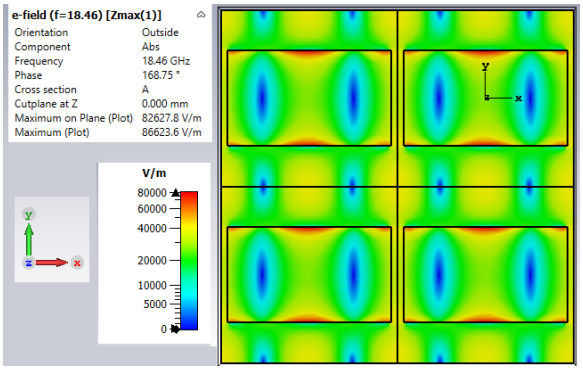

Fig. 5. Text text text text text text text text text text text. (a) Text text text. (b) Text text text text.

Figures 6 and 8 display the full-wave field distributions for the yellow-point device at a thickness of $L_z = 0.375\,\text{mm}$ and $\theta = 0.5°$, computed using 40 Bloch-Floquet modes—comprising 20 S-polarized and 20 P-polarized modes—corresponding to the resonance at $f = 18.46\,\text{GHz}$ and the BIC

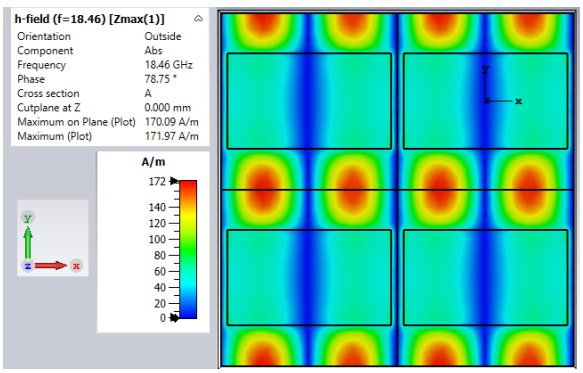

Fig. 6. Text text text text text text text text text text text. (a) Text text text. (b) Text text text text.

at the highest frequency of $f = 18.855\,\text{GHz}$, respectively, as depicted in Figure 3. The field distributions at the midpoint cross-section, $z = 0$, demonstrate the influence of a large perforated window area within the silicon background.

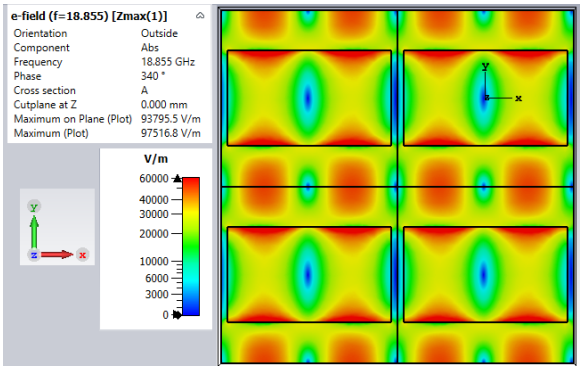

Fig. 7. yyyyyy

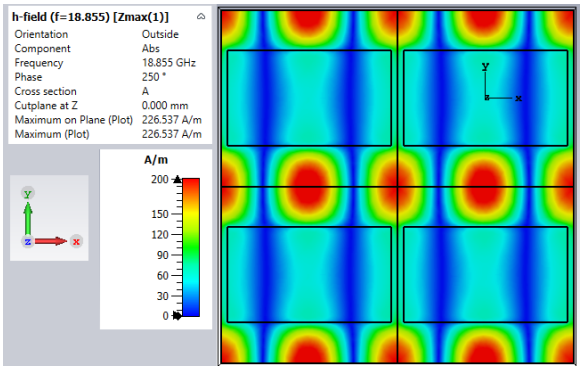

Fig. 8. Text text text text text text text text text text text. (a) Text text text. (b) Text text text text.

The full-wave plots are derived from $\Re[\vec{H}e^{-iu}]$, where the total magnetic field $\vec{H}$ is expressed as $\vec{H} = \vec{H}_{(0,0)} + \sum \vec{H}_{\text{BF}\neq(0,0)}$, representing its decomposition into components. The phase u is an adjustable parameter, chosen to suppress the influence of the incoming propagating mode $BF_{(0,0)}$ such that $\left|\Re[\vec{H}_{(0,0)}e^{-iu}]\right| \approx 0$. This method is applicable at normal incidence ($\theta = 0, \varphi = 0$) and, consequently, extends to our scenario, which closely approximates normal incidence. The obtained plots illustrate the C_4 symmetry in the contribution of the excited evanescent modes associated with these quasi-BICs.

IV. Conclusions

References

[1] J. von Neumann and E. Wigner, "Über merkwürdige diskrete Eigenwerte. (English) [On unusual discrete eigenvalues]," *Zeitschrift für Physik*, vol. 30, no. ??, pp. 465–467, ???? 1929, reprinted in [6, Paper 23].

[2] H. Friedrich and D. Wintgen, "Interfering resonances and bound states in the continuum," *Physical Review A*, vol. 32, no. 6, p. 3231, 1985.

[3] B. Zhen, C. W. Hsu, L. Lu, A. D. Stone, and M. Soljačić, "Topological nature of optical bound states in the continuum," *Physical review letters*, vol. 113, no. 25, p. 257401, 2014.

[4] O.-Z. Lipan and A. De Sabata, "Closed-form analytical solution for the transfer matrix based on Pendry-MacKinnon discrete Maxwell's equations," *Optics Express*, vol. 33, no. 3, pp. 3777–3817, 2025.

[5] ——, “Bound states in the continuum via singular transfer matrices,” *Physical Review A*, vol. 111, no. 3, p. 033516, 2025.
[6] A. H. Taub, Ed., *John von Neumann: Collected Works: Volume I: Logic, Theory of Sets and Quantum Mechanics*, 1961.